SIZE AND SHAPE-BASED SEPARATION USING DETERMINISTIC LATERAL DISPLACEMENT MICROFLUDIC SYSTEMS

By

MINGLIANG JIANG

A thesis submitted to the

Graduate School-New Brunswick

Rutgers, The State University of New Jersey

In partial fulfillment of the requirements

For the degree of

Master of Science

Graduate Program in Mechanical and Aerospace Engineering

Written under the direction of

[German Drazer]

And approved by

_____

_____

_____

New Brunswick, New Jersey

October, 2014

ABSTRACT OF THE THESIS

Size and shape-based separation using deterministic lateral displacement microfluidic systems

by MINGLIANG JIANG

Thesis Director:

German Drazer

Continuous separation of particles of different sizes and shapes is important in both clinical diagnostics and industrial applications and a number of methods have been developed for such separations. In microfluidic systems, deterministic lateral displacement has proved its great potential in achieving the goal of high throughput and efficient separation. Although it was originally based on transporting the suspension in a convective flow, particles can be also driven with external force fields, thus force-driven DLD (f-DLD) devices were demonstrated. This thesis demonstrates the separation of suspended particles by shape and size using scaled-up macroscopic f-DLD devices, using gravity force and a centrifuge, respectively.

In the first set of experiments and for the first time, we demonstrate the potential of gravity-driven DLD devices for the separation of particles of different shapes. Our results show that each type of particle moves in different directions within the array of obstacles in DLD systems, depending on the forcing direction. Interestingly, we show that the migration of the particles can be predicted by the diameter of the inscribed sphere, independent of shape.

In the second set of experiments and also for the first time, we combined DLD

devices with centrifugal force as the driving field. We show that spherical particles of different sizes are driven to different outlets. We show that at some specific angles this setup provides high separation resolution, but the resolution decreases as the concentration of particles increases.

Acknowledgement

This thesis would not have been possible unless my advisor, Dr. German Drazer, encouraged, guided and supported me in all my time of research and writing of this thesis. I am grateful to work under the supervision of such a far-sighted, patient, highly-motivated, knowledgeable and enthusiastic scientist. I joined the Microfluidics Laboratory in the fall of 2012. I was afforded the precious opportunity of working in immediate collaboration with my principle investigator. Dr. Drazer offered me numerous ideas in research. This experience has helped cultivate my ability to do design experiments and dealing with data and for these, I am greatly indebted.

I would also like to express my sincere gratitude to my family for their continued support throughout my two years at Rutgers University. I am very grateful for having such accommodating parents, Jiabao Jiang and Ling Liu, and I hope the work contained herein makes them proud. Additionally, I thank my labmates, Kostyantyn Budzan and Parth Patel, two genius undergraduates who cooperated with me on two different projects respectively.

Table of Contents

List of Tables

List of Illustrations

Introduction

Microfluidics is an interdisciplinary science that intersects engineering, physics, chemistry, biotechnology and has a large number of practical applications to the design of systems or devices which manipulates minute volumes of liquid. Fabrication techniques produce micro devices such as lab-on-a-chip (LOC) devices at a high precision.[1] A lab-on-a-chip (LOC) is a device that integrates one or several individual unit operations on a single chip of only millimeters to a few square centimeters in size handling extremely small fluid volumes. Lab-on-a-chip devices are also often indicated by "Micro Total Analysis Systems" (μTAS). Integration of microfluidics with micro total analysis systems (μ-TAS) or Lab-on-a-chip (LOC) can provide high throughput, reduce cost per analysis and outside contamination or human involvement[2]. Fig.1 shows one of the first integrated DNA analysis systems, which is composed of microfabricated fluidic channels, heaters, sensors and detectors. These components operate as a single closed system and have the potential to analyze DNA at low unit cost. Over the past few decades, microfluidics has evolved into a powerful technology within a wide range of biological areas such as DNA chips[3], drug delivery[4], fuel cells[5], medical diagnostics and biosensors[6], cell analysis[7], and microreactors[8]. Although microfluidic technology has become more and more impactful in the real world, there is still a lot to be explored in the field of lab-on-a-chip.

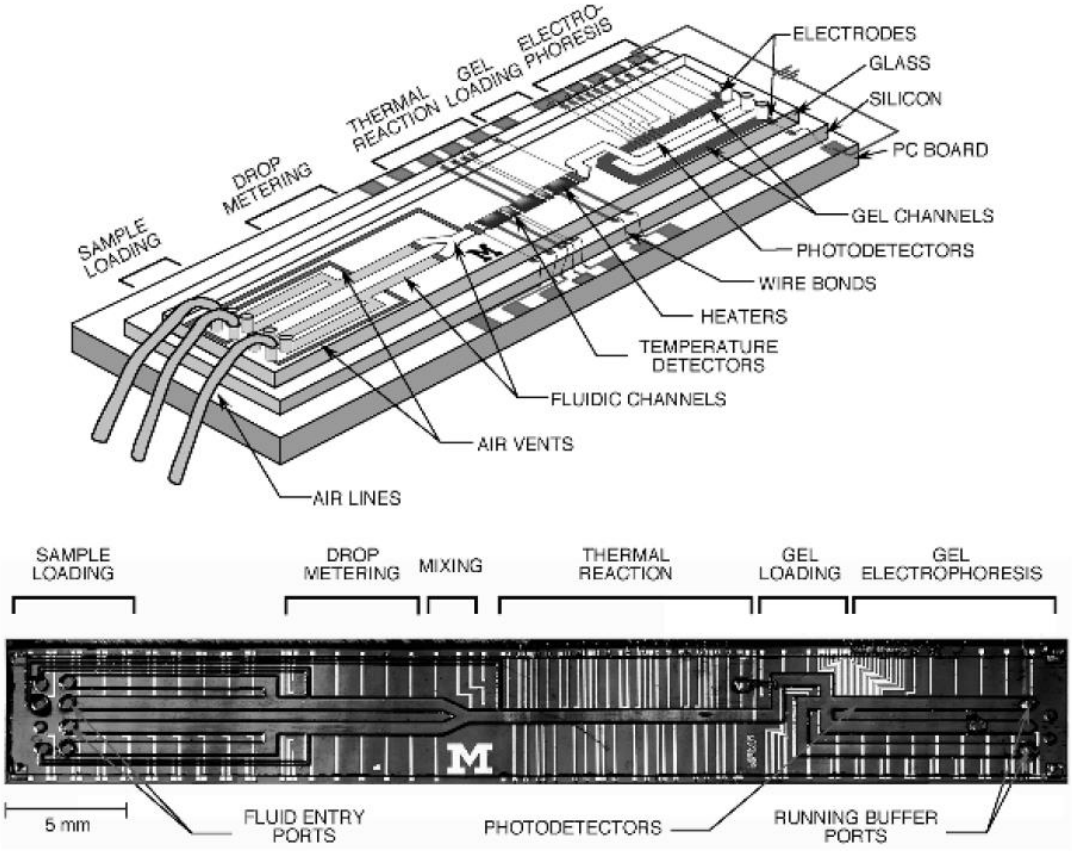

Fig.1 Integrated DNA analysis device developed by Burns *et al.* in 1998. This integrated device contains microfabricated components such as heaters, sensors, and channels, capable of analyzing DNA without external lenses or heaters. Image reproduced from "An Integrated Nanoliter DNA Analysis Device".[9]

The ability to separate cells and particles with high resolution is central to the development of μ-TAS or LOCs as usually analytical systems need to separate different species before analysis.[10] A significant number of methods have been developed to separate particles or cells in microfluidic systems based on their intrinsic physical properties including size, shape, density, electrical, and optical properties since microfluidic devices could greatly reduce cost while also provide high throughput. Externally induced forces such as optical, dielectric, magnetic and acoustic forces are also introduced to the micro domain to drive particles or cells in complex mixtures[11]. Typically, there are two types of separation techniques: active

ones, which involve external fields and passive ones, without utilizing any external force. For the active separation methods, there are flow filed fractionation[12], split thin flow fractionation[13], optical methods[14], dielectrophoresis[15], magnetropheresis[16], and acoustophoresis[17]. As to the passive ones, there exist deterministic lateral displacement[18], hydrodynamic filtration[19], pinched flow fractionation[20], and inertial and dean flow[21]. First proposed by Huang *et al*[18], deterministic lateral displacement is considered as one of the most typical passive strategies. The separation device is composed of an array of micro posts or obstacles on a lattice board where obstacles are used to alter the streamlines or particle trajectories.

This thesis focuses on separation of particles in DLD microfluidic devices. When particles are driven though an array of obstacles on a plane, they collide with obstacles and change their directions. Particles of different sizes follow trajectories with a different orientation in average and thus they are separated. Fig.2 shows two typical trajectories in a DLD device. Smaller particles move closer to the flow direction and cross one column of obstacles after every few rows (the green trajectory in the figure). This type of motion is usually called “zigzag” motion. On the other hand, larger particles move along a column of obstacles and do not cross it, which results in a larger migration angle between its path and the flow direction. This type of motion is usually called “displacement” motion.

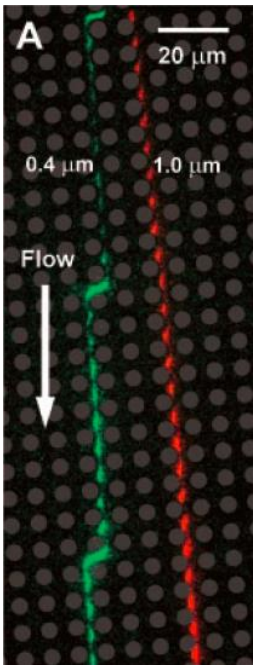

Fig.2 Image of the first DLD separation device. The 0.4 μm green fluorescent tagged particles on the left follow a "zigzag" motion while the larger 1.0 μm red fluorescently tagged particles on the right travel in a "displacement" mode. Image reproduced from Huang *et al*.[18]

A significant amount of research has been done in separation of rigid particles in deterministic lateral displacement devices, mostly focusing on size separation. For instance, Raghavendra Devendra *et al* applied gravity to drive particles of different sizes through a DLD device[22]. In addition, new designs of arrays in DLD are developed to improve the separation efficiency. Triangular posts have been proposed to improve the separation as compared to the use of circular posts.[23] Al-Fandi *et al* proposed airfoil and diamond posts and demonstrated that airfoil posts has the potential to overcome complication and deformation of soft biological particles[24]. DLD devices have also proved their potential for separation of non-spherical and deformable bioparticles[25,26,27].

In deterministic lateral displacement devices, particles follow a predetermined (deterministic) trajectory, which means this method does not rely on a random process

for the separation process. In addition, this technique has some other advantages such as high throughput, fast speed, and low energy consumption. However, it also has some limitations. First, it is not easy to solve the clogging problem. Second, it requires a high accuracy in the fabrication of micro devices as all the parameters such as gap and diameter of obstacles have to be the same throughout the system, otherwise the resolution would be low. Therefore, the fabrication yield for these devices might be low.

The purpose of this essay is to experimentally demonstrate the potential of DLD devices for both size- and shape-based separation and the effects of combination of passive DLD devices with gravity force or a centrifuge on particle separation. Our group has numerically explored the underlying mechanism of separation in DLD devices[28,29,30] and experimentally investigated the feasibility of force-driven DLD (f-DLD) devices, mainly gravity-driven DLD (g-DLD), in separation of particles of different sizes in macroscopic systems as well as microfluidic devices[22,31]. In Part A of the thesis, for the first time, we demonstrate that g-DLD could also be used to separate particles of different shapes. In Part B, for the first time, centrifugal force is introduced to DLD systems for separation.

Discussion of macroscopic experimental setup

Since DLD originated from microfluidic systems, it is necessary to justify the use of scaled up macroscopic devices in our experiments. We decided to use

macroscopic systems as it provides easy to operate experiments, allows us to reuse the same system, and it is straightforward to capture the details of particles motion.

In previous experiments performed in our group, the aspect ratio of devices are held constant and dimensionless numbers related to fluid motion are maintaned the same. The two main dimensionless numbers are *Re* and *Pe*. The Reynolds number is the ratio of fluid inertial force to viscous force, given as

$$Re = \frac{\rho_f U l_c}{\mu} \tag{1}$$

Where in our experiments, ρ_f is the fluid density, U is the particle velocity, l_c is a characteristic length of the particle, and μ is the dynamic viscosity of the fluid. In previous studies, we have maintained a low Reynolds number and shown their consistency within microscopic environments[22,31]. In our experiments, we even simplified the system by using water as the fluid and thus leading to a relative larger Reynolds number. While the number is still O(100) or smaller. The Péclet number relates the ratio of the rate of advection to the rate of diffusion, expressed as

$$Pe = \frac{U l_c}{D} \tag{2}$$

Where D is the diffusion constant of the particle in the fluid and l_c is the characteristic length of the particle. When the Péclet number is very high (Pe » 1), Brownian motion can be neglected. All DLD systems function at a high Péclet number.

Experimental setup and discussion of force-driven DLD devices

A. Separation of particles of different sizes and shapes by gravity force in Deterministic lateral displacement devices

Introduction

The separation of particles from a mixture has an essential biological, medical and industrial application such as blood cells sorting[27]and separation of nanometer gold particles[32]. Shape and size are considered as two main physical properties for recognizing bioparticles or nanoparticles[33]. Shape is an important clinical indicator, for instance, red blood cells have different shapes in different diseases thus it provides us a relatively convenient method to diagnose diseases by measuring the shape of red blood cells[34]. In addition, cells have various shapes and sizes at different life stages so that it's easy to identify them and synthesized nanoparticles also show size[35] and shape dependent properties[36].

Recently, more and more work has been done to explore the potential capability of some well-established size-based separation techniques for shape-based separation. Wei *et al* first reported the capability of size-exclusion chromatography for the shape separation of gold nanoparticles since this technique was considered as size based[32]. Sugaya *et al* successfully separated spherical and non-spherical particles using hydrodynamic filtration scheme[37].

In this thesis, we separated rigid particles of different sizes and shapes with a combination of a DLD device and gravity force in a scaled-up device. It is the first time that f-DLD is applied to separate particles of different shapes. We adjust the forcing angle (α) of the experimental setup to find the relation between the forcing

angle and crossing probability (P). The forcing angle is defined by the direction of gravity force with respect to the array of obstacles which is shown in Fig.3. Thus, 0°, for instance, means the column of obstacles is aligned with the gravity. The crossing probability is the number of particles which crossed any column of obstacles over all the "effective" particles we counted. The effective particles are the particles that moved throughout the device, without becoming trapped at some obstacle. We also found out the relation between the critical angle (Θ_c) and some specific diameter or volume for each particle. Here the critical angle is defined as the forcing angle at which the particles move across columns of obstacles and migrate at an angle different from zero. Since not all the particles of a given species will cross at the same angle, we defined it as the forcing angle at which half of the particles crossed any column of obstacles. When the particles move across columns of obstacles, we say it migrated. As shown in Fig.5, the blue particles migrated while the green ones did not. In addition, we obtained the rectilinear path of a particle by connecting its inlet and outlet to the lattice board with a straight line and we measured the migration angle (β), which is defined by the direction of the path of a particle with respect to the direction of the gravity force.

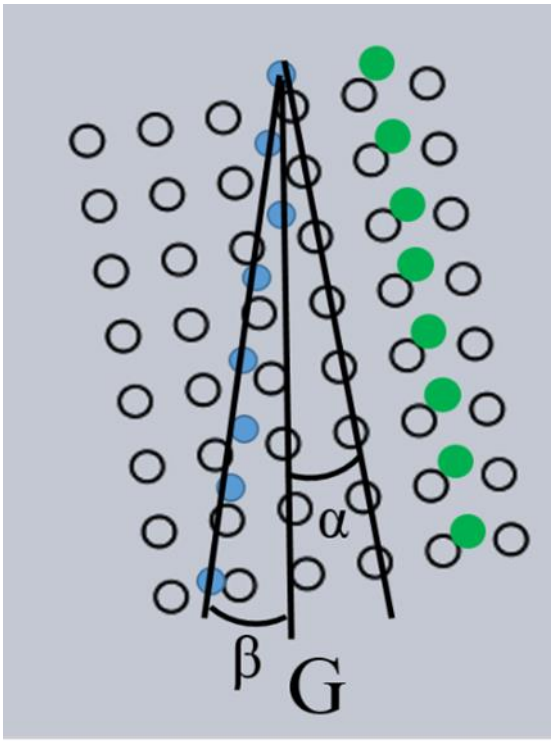

Fig.3 Schematic view of particles' motion in DLD and some specific angles. α is the forcing angle, β is the migration angle, G is gravity. Blue particles cross a few column of obstacles, they migrate and green particles do not cross any column of obstacle, they are locked.

Experimental setup

The separation system is composed of three parts: the plastic bottom board, the cover glass and the lattice board. We fabricated the lattice board 200mm x 200mm made of VeroWhite Plus with a 3D printer. There are 35 x 35 cylindrical posts on the lattice board. The diameter of the obstacle (2R) is 1mm and the spacing between two adjacent obstacles is 5mm. The board is set inside the recess of a plastic bottom board and covered by a piece of acrylic glass. It is immersed in water and lined up vertically so that gravity is in the same plane with the arrays. We created a trench or groove on the bottom board and fill it with an O-ring for sealing. Then we covered them with a glass plate. A valve was set at the bottom of the system and it is used to drain water

and collect particles. We finally mounted the separation system on a rotating disk such that we could adjust the angles conveniently. The rotation system is composed of a base and a round disk. The whole system is shown in Fig.4.

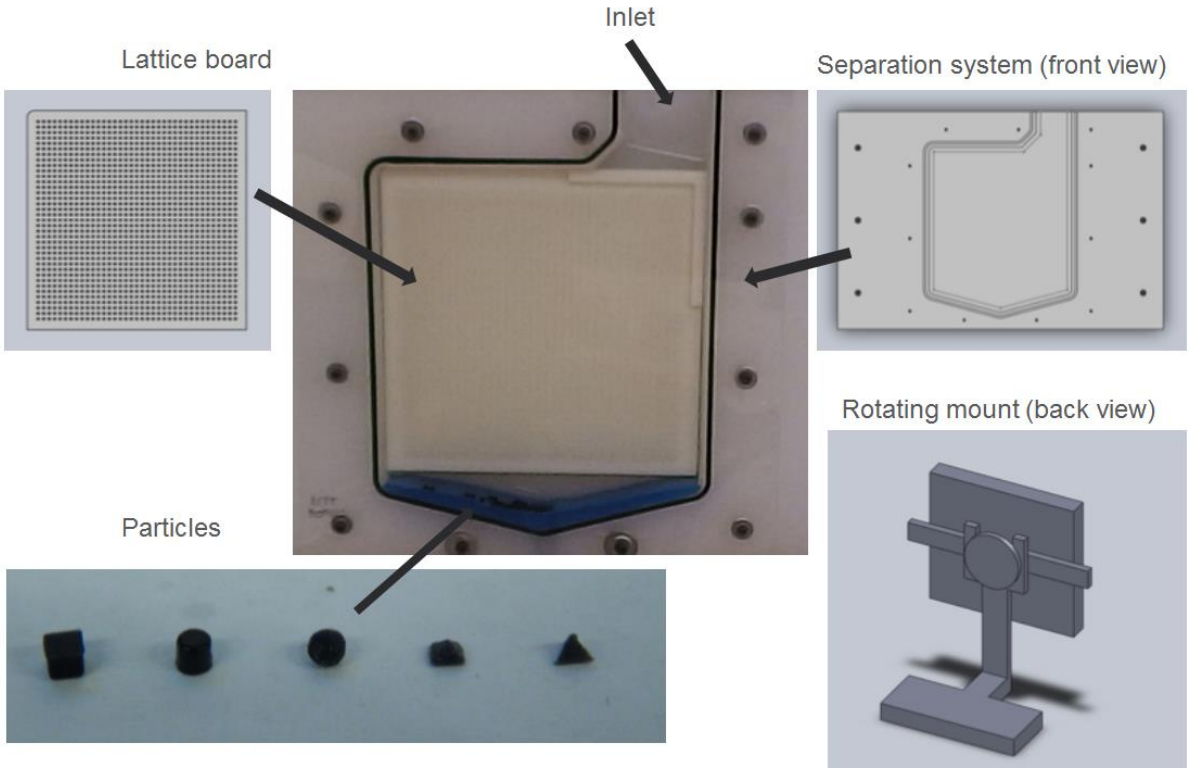

Fig.4 The separation system and rotation system for g-DLD devices.

We printed out particles of different shapes, including cubes, cylinders, pyramids, spheres and tetrahedrons. They are made of TangoBlack® material which has a density of 1.13g/cm3. Here we use the size of a characteristic dimension of the particles as the nominal size *a*. According to Bowman *et al*'s work[28], larger aspect ratio of particle size to the obstacle diameter ($a/2R>1$) corresponds to a better resolution. Besides, we noticed that smaller particles whose diameter is less than that of the cylindrical posts were usually stopped by the obstacles during the migration process and could not move any more. Also enough space is needed to allow the

biggest particles to pass the gap between the adjacent obstacles. The sizes of the particles we used are shown in Table 1. The particles are shown in Fig.4.

Size(mm) / Shape	1.50	1.75	2.00	2.25	2.50	2.75	3.00	3.25	3.50
Cube	●	●	●	●					
Cylinder			●	●	●	●			
Pyramid			●	●	●	●			
Sphere			●		●	●	●		
Tetrahedron			●		●		●		●

Table 1. Particles used in g-DLD devices. Cells with a dot inside indicate the corresponding type of particles was used in experiments

Since the sides of the plastic board and the lattice board are parallel, and the latter is fixed inside the former, we adjust the forcing angle of the lattice board by rotating the plastic board.

We performed experiments in the following way. The lattice board is lined up vertically so that the gravity is in the plane of the array. We released the particles from the top of the tank. The gravity drives them through the array of cylindrical obstacles. We rotated the tank to adjust the forcing angles to the desired values. We did one hundred trials for each type of particle. At the end, we opened the valve at the bottom of the tank, filtered the water and collected the 100 particles. We recorded the whole process and tracked the particles by ImageJ.

Results and discussion

We plot the crossing probability, P, as a function of the forcing angle, α.

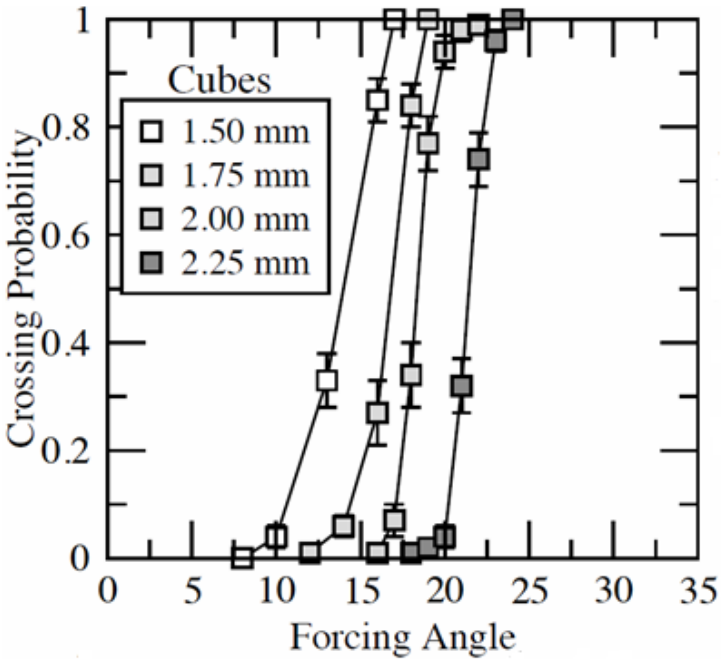

Fig.5 (a)

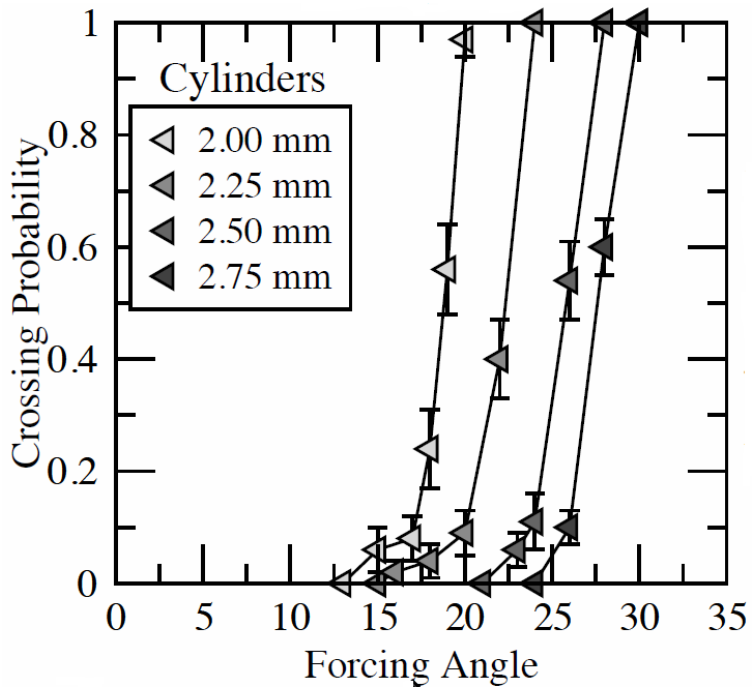

Fig.5 (b)

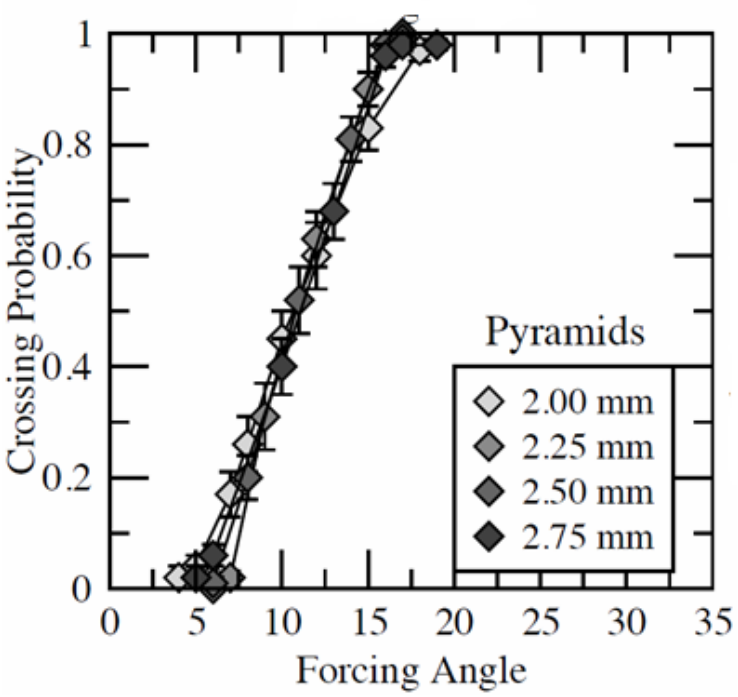
Crossing Probability
Forcing Angle
Pyramids
2.00 mm
2.25 mm
2.50 mm
2.75 mm
0
0.2
0.4
0.6
0.8
1
0
5
10
15
20
25
30
35

Fig.5 (c)

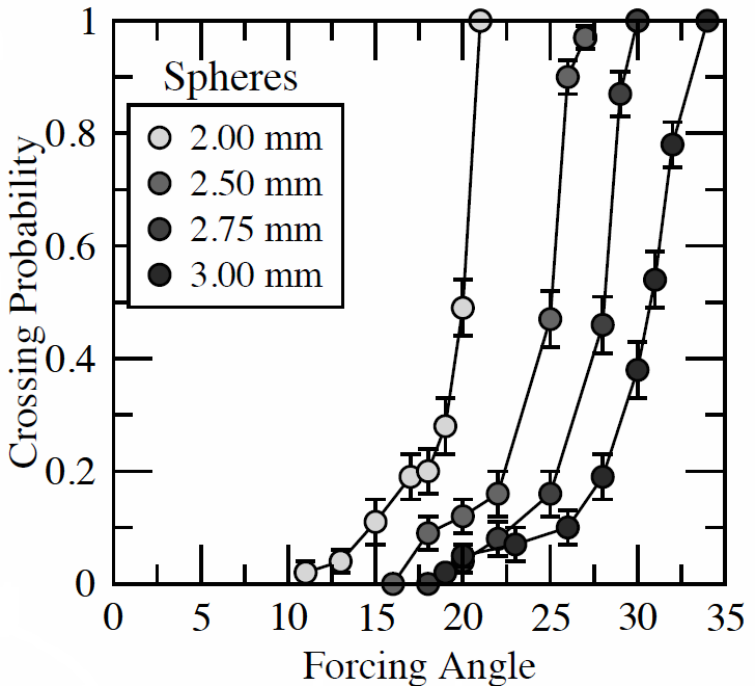
Crossing Probability
Forcing Angle
Spheres
2.00 mm
2.50 mm
2.75 mm
3.00 mm
0
0.2
0.4
0.6
0.8
1
0
5
10
15
20
25
30
35

Fig.5 (d)

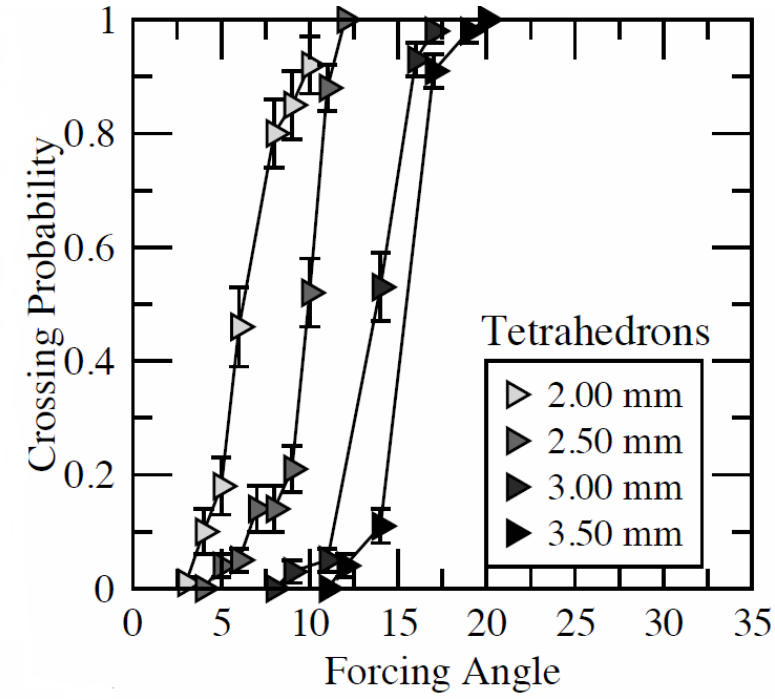

Fig.5 (e)

Fig.5(a)~(e) The crossing probability as a function of forcing angle for cubes, cylinders, pyramids, spheres and tetrahedrons. The curves are like staircases. They increase very slowly at the beginning, which means very few particles migrate when forcing angles are small. But then they increase very fast after some specific angles, and at last become flat.

As shown in Fig.5 (a)~(e), in each type of particle, as the forcing increases, the probability increases, that is, more and more particles move across individual columns of obstacles in the device. Generally, we observe S-shaped curves for the crossing probability. At the beginning, only a few particles migrate. Again, the term ‘migrate’ is referred here as the particles crossing any column of obstacles. The curve goes up very slowly for the first few forcing angles. Then suddenly the probability increases relatively fast. Especially for cubes and cylinders, their probability curves are quite sharp. At the end, all the particles migrate and the curves become flat. Each plot shows a comparison of the same shape of particles for different nominal sizes. It is clear that as the nominal size increases, the starting forcing angle at which some particles migrate also increases, which means the larger the particle is, the larger the

angles needed for it to migrate. This helps us separate them at some specific angles. Only the pyramidal particles seem to migrate in the same range of forcing angles independent of their size, which would make it extremely difficult to separate them.

As shown in Fig.5 (a), for cubes of 1.50mm, all particles are locked before the starting angle of almost 8 degrees. As the forcing angle increases, more and more particles begin to migrate. At forcing angles around 17 degrees, all the particles have migrated. There is a sharp increase between the starting and ending forcing angles. As the size of cubes increase from 1.50mm to 2.25mm, the probability curves move right, that is, the staring forcing angle at which particles migrate increases. Similar behavior is observed for the other shapes, except the case of pyramids. This behavior is in agreement with what was observed in previous macroscopic experiments using spherical particles, in which a clear transition angle was observed. It is also in agreement with the case of spherical particles in microfluidic experiments, in which case we also see a sharp transition at a critical angle[30].

However, there is a small difference with past experiments for the case of spherical particles in macroscopic systems. In previous experiments the transition takes place at a given angle, there was almost no measurable width of the transition. We believe that this difference is due to the presence of inertia effects in the present experiments. Moreover, the velocity changes as the angle approaches the transition angle, and the magnitude of inertia forces is, therefore, also changing. In order to determine if the observed broader transition is in fact due to inertia, we performed a second set of experiments in which we increased the viscosity of the fluid. We

obtained the more viscous fluid by mixing 50% water and 50% glycerin in volume. In this case, the entire probability-forcing angle curve shifts left and, as expected, the transition becomes significantly sharper, as can be seen in Fig.10.

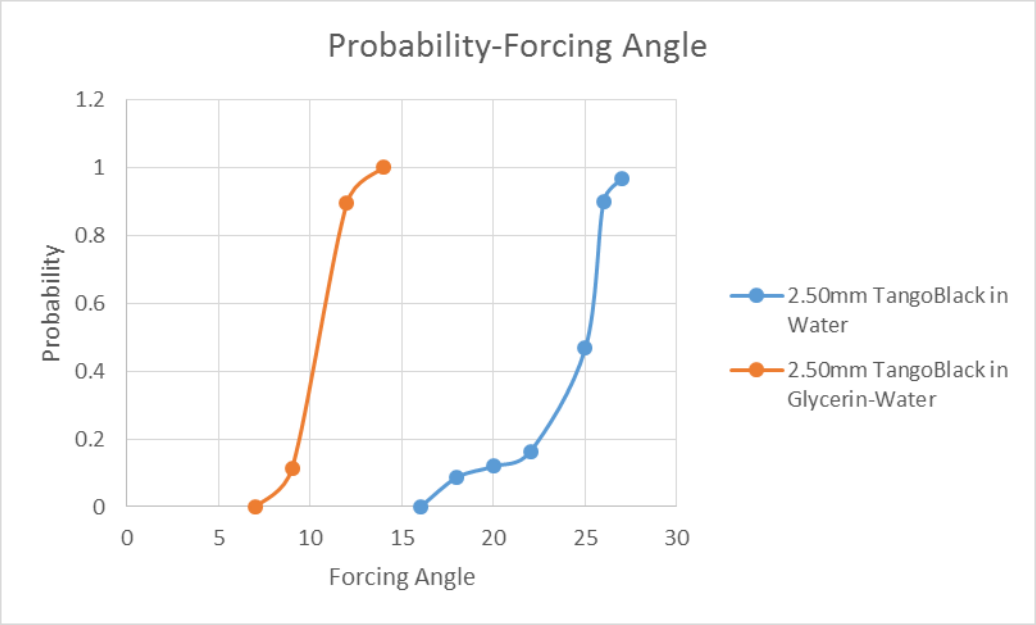

Fig.6 The crossing probability as a function forcing angle for 2.50mm Tangoblack particles in water and water-glycerin. Water glycerin is 50% glycerin and 50% water mixed in volume.

We also plot the critical angle as a function of different characteristic sizes of a given particle shape, in an effort to find a *universal* way to describe the relation between the critical angle and the size. That is, one characteristic length that provides the same size-vs-transition angle curve, independent of the shape of the particle. The nominal size is the length of each side of a particle. The inscribed sphere is the largest sphere that is contained inside a given particle (polyhedron) and tangent to each of the polyhedron's faces. The circumscribed sphere is the smallest sphere which contains the polyhedron and touches each of the polyhedron's vertices. The critical angle of the different types of particles as a function of these characteristic lengths, that is the

diameter of the inscribed sphere, the diameter of the circumscribed sphere and the nominal size, are shown in Fig.7 (a)~(c).

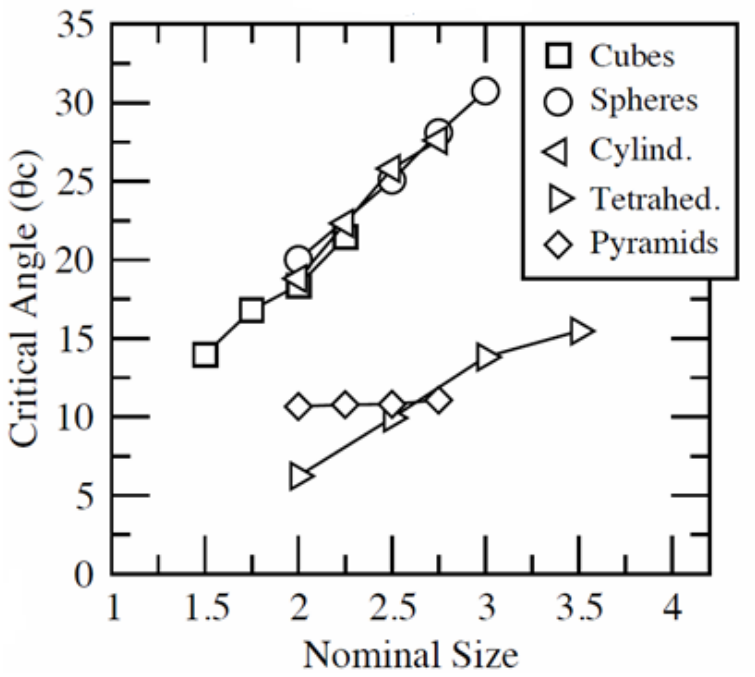

Fig.7 (a)

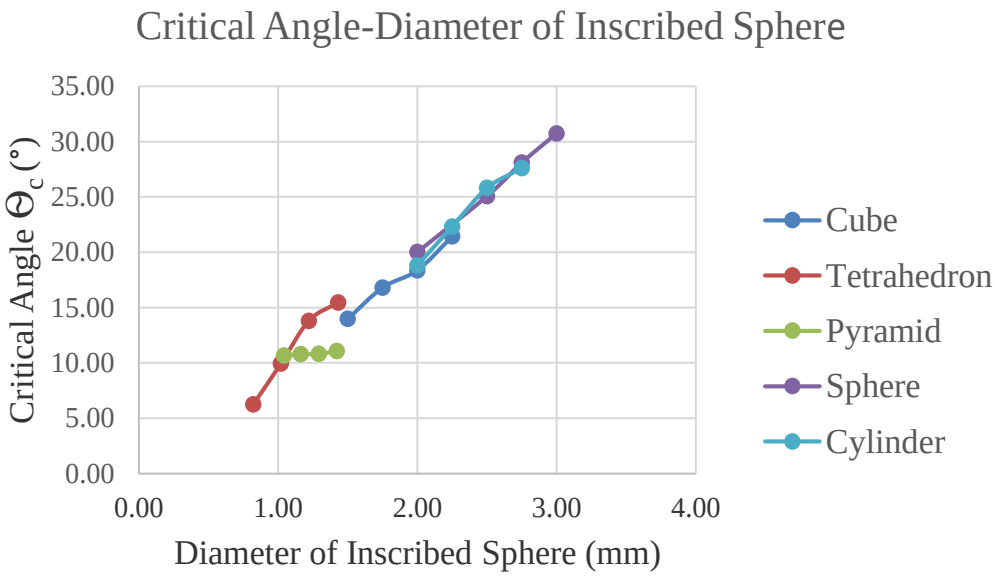

Fig.7 (b)

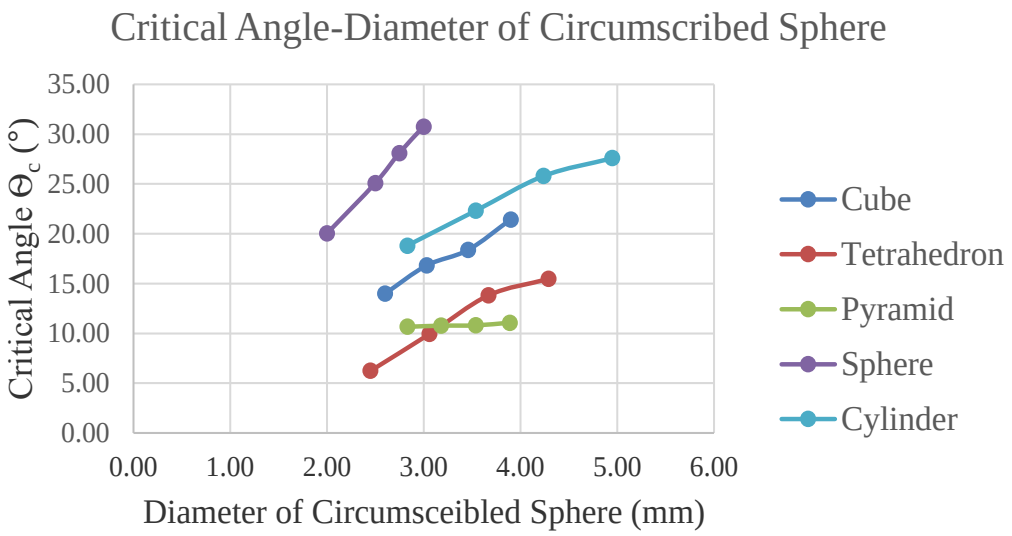

Fig.7 (c)

Fig.7 (a)~(c) The critical angle as a function of nominal size, diameter of inscribed sphere and diameter of circumscribed sphere of particles. The relations between the critical angle and the sizes are almost linear.

As shown in figure 7, as the size increases, the critical angle increases. In Fig.7 (a), the curves of cubes, cylinders and spheres seem to overlap with each other. In Fig.7 (b), all the curves follow a linear trend except pyramids. In Fig.7 (c), all of them are separated.

Firgure 7c shows that the diameter of inscribed sphere provides a relatively good collapse of all particles, including the case of pyramidal particles, and it is therefore an important factor to decide whether two types of particles of different shapes could be separated. For example, it's very hard to separate spherical particles which has a nominal size of 2.00mm and cubic particles which has a nominal size of 2.00mm since they behave similarly.

We also plot the average migration angle, β_{AM}, as a function of forcing angle, α, as shown in Fig.8.

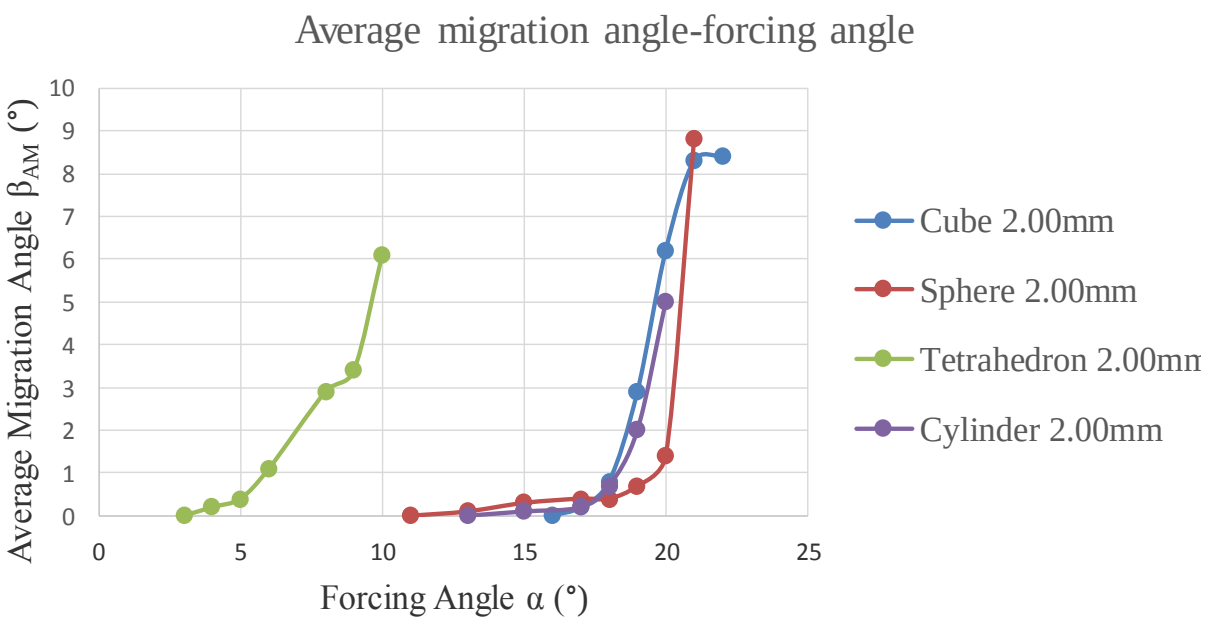

Fig.8 Average migration angle as a function of forcing angle. The curves rise suddenly after some specific forcing angles.

As the forcing angle increases, the average migration increases. At the beginning, it increases very slowly, but after a certain angle, it rises all the way to the top very fast and ends suddenly. The curves have a "J-shape". Only the tetrahedral particles curve is separated from the other types of particles while the other three curves seem to overlap each other (Note that we did not perform these experiments for pyramidal particles).

Conclusions

We have shown that gravity-driven deterministic lateral displacement (g-DLD) has a great potential for separation of particles of different shapes and sizes which has a great application in clinical diagnostics especially in recognizing and separating bioparticles or cells. We performed experiments in a scaled-up device consisting of an array of cylindrical posts. We investigated the relation between the

crossing probability and the forcing angle. Our results have shown that each type of particle starts to migrate at a given forcing angle. As the forcing angle increases, more and more particles migrate until at last all of them finally move across obstacle columns and move at angles different from zero. For the same shape of particles but different sizes, they start to migrate at different forcing angles. As the size increases, the starting forcing angle increases. We plot the critical angle as a function of several characteristic dimensions of a particle such, as the nominal size, diameter of inscribed sphere and diameter of circumscribed sphere. We noticed that diameter of inscribed sphere is an effective factor to separate particles of different shapes. Thus, particles of different shapes which have similar diameter of inscribed sphere will not be separated easily. We showed the relation between the average migration angle and forcing angle for different shapes of particles at the same nominal size. The average migration angle increases with the forcing angle slowly at the beginning and the pace suddenly changes after a small increase in the forcing angles. We observed that as the viscosity of the fluid we filled in the tank increases, the "probability-vs-forcing angle" curves shifts left, which means the particles tend to migrate earlier in more viscous fluids, and the curves becomes sharper, which means the particles transition from *displacement* to *zigzag* mode faster and would provide higher separation resolution. More work will be done to investigate the relation between the shape of the "probability-vs-forcing angle" curve and the viscosity of the fluid medium. Finally, we would like to point out that changing the value of some parameters could be interesting, thus providing directions for future separation work within this type of

set-up, i.e., increasing of the spacing between obstacles and decreasing of the diameter of cylindrical obstacles may effectively solved the problem of clogging and impediment (particles being trapped before exiting the system) in the device.

B. Separation of spherical particles of different sizes by a centrifuge in deterministic lateral displacement devices

Introduction

Centrifugal force has been widely used in separation of cells or particles in microfluidics since it is fast, powerful and easy to operate. Recently, more and more efforts have been put to combine DLD with external force fields to improve separation efficiency. Devendra *et al* applied gravity to drive particles of different sizes through a DLD device[22]. Beech *et al* experimentally demonstrated and numerically investigated the feasibility of combination of dielectrophoresis and DLD in separation of particles[38]. Another advantage of incorporating external forces is that it might help reducing the trapping of particles inside the array of obstacles.

In this thesis, we first combined DLD with centrifugal force which can overcome the trapping and potential clogging problem of DLD, by forcefully decreasing the interaction time between obstacles and particles and/or removing trapped particles by increasing the external force. Based on our previous experience in application of gravity force in scaled up DLD devices, we also performed experiments in a macroscopic environment. The Reynolds number in this scaled up system was maintained very low, even less than 10.

Experimental setup

The centrifugal force-driven DLD experimental setup consists of a separation device, a centrifuge which is used to drive particles, a computer which is used to receive signal of experiments, a tachometer which is used to read the rotation speed of the centrifuge and transfer signal to the computer, a high speed camera which is used to capture the motion of particles and transmit data to the computer. The work principle of this system is as follows: the red laser was sent out by the tachometer and projected to the edge of the center of the centrifuge. A reflection tape was attached to the edge of the center of the centrifuge. The tape reflected the red laser back to the tachometer every time it passed. Thus the tachometer read the speed of the centrifuge and sent the reflection signal to the computer. Then the computer directed the high speed camera to take one picture of the device each time. In this way the pictures are synchronized and show the same position of the device with respect to the lab reference frame. These pictures were sent back to the computer and the trajectory of the particles can then be calculated.

The separation device is composed of four major parts: a lattice chip, a chip house, a rotation board and a base. The size of the lattice chip is 59x39mm. There are 12x10 cylindrical obstacles placed on it. The diameter of the obstacles is 0.5mm, the height of the obstacles is 3.0mm, and the spacing between the centers of two adjacent obstacles is 3.5mm. A dividing wall was created on the upper left corner of the chip in order to position the particles at the beginning of the experiments. We released particles at the upper left corner of the top wall and the right side of the release bar,

which is shown in Fig.9. We built ten bars at the bottom of the lattice chip. Thus eleven outlets were created for particles collection.

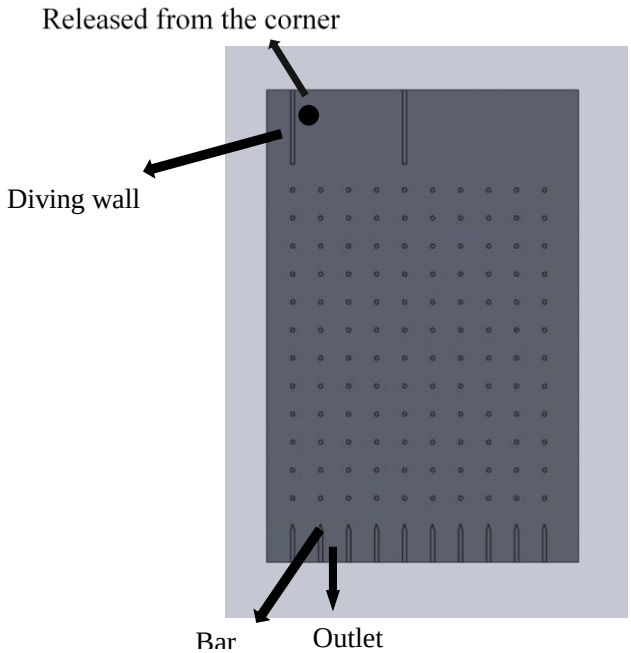

Fig.9 Schematic view of the lattice board for centrifuge-DLD devices. Particles were released from the upper left corner. They were driven through the entire device and collected at the outlets.

The separation device is shown in Fig.10. We embedded the lattice chip into the chip house and then fixed the chip house to the rotation board. We drilled 20, center-symmetric holes in total on the rotation board, with a spacing of 5 degrees. And we also drilled two holes on the base, of the same size as the holes on the rotation board, which are used to connect the rotation board. Thus we could adjust the angles from 0 to 45 degrees with an increment of 5 degrees by selecting the appropriate hole to connect the rotation board to the base. The base is set on the rotation board of the centrifuge, thus the whole separation device is fixed to the centrifuge. The rotation speed of the centrifuge in steady state is around 600 rpm.

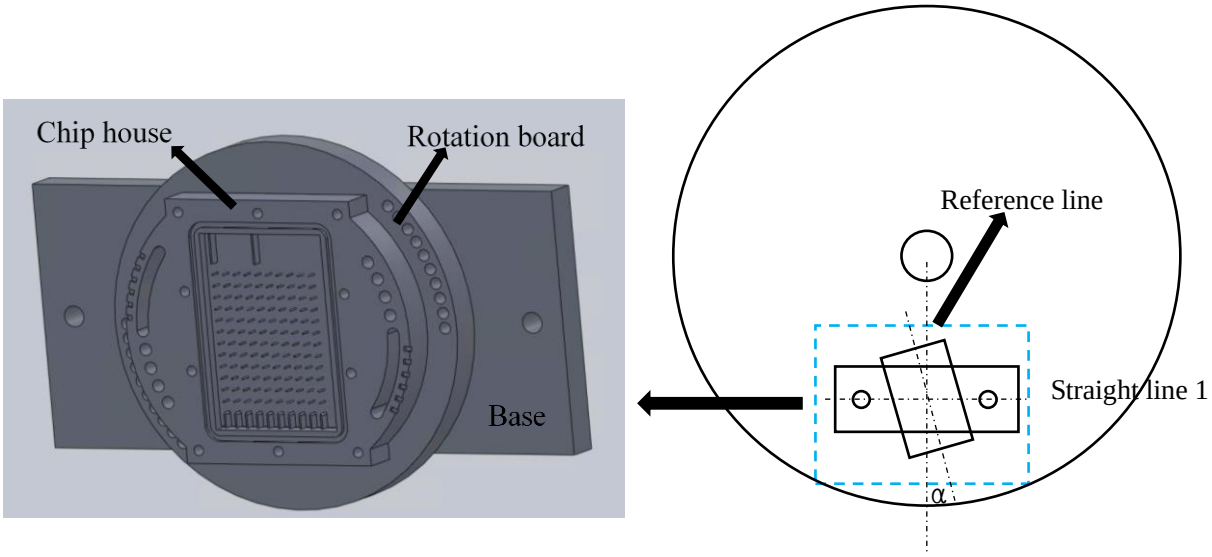

Fig.10 Schematic view of the separation system for centrifuge-DLD devices. α is the forcing angle, it is the angle between the reference line and a column of obstacles. The two big holes on the base of the separation device are symmetric, we connected their centers and obtained a straight line 1. Then we drew another straight line 2 which is vertical to line 1 and found their intersection. We made all the four components concentric at this point. The straight line 2 is considered as a reference line. Thus the forcing angle was obtained by measuring the angle between a column of obstacles and this reference line.

We adjusted the forcing angle (α) of the experimental setup to find the probability distribution, P_i of particles exiting the device in outlet I, at a specific forcing angle. The forcing angle is defined as the angle between a column of obstacles and the reference line which is shown in Fig.1. Thus, 0°, for instance, means the column of obstacles is aligned with the reference line in the direction of the driving force. The probability is the number of one type of particles which were collected at an outlet over all the "effective" particles of this type that we tracked. The effective particles are the particles that did not get stuck during their motion. We compared the separation results at different forcing angles. We also investigated the effect that the number of particles released together has on the probability distribution.

We used two types of spherical particles: cellulose acetate particles (1.26g/cm^3) and Delrin® acetal particles (1.41g/cm^3). We picked the size of particles

and design parameters of the lattice board from our previous experience in experiments with gravity driven DLD devices. For the cellulose acetate particles, their diameters are 1.00mm and 1.50mm. For Delrin® acetal particles, their diameters are 1.59mm and 2.38mm.

We performed the experiments as follows. First, we set an equal number of particles of two different sizes at the upper left corner between the top wall of the chip house and the right side of the dividing wall. For example, among four cellulose acetate particles, two are big and the other two are small. We grouped them together without deliberately setting the relation between their positions and called this position as "group placement". We started the centrifuge and the particles were driven through the array of cylindrical obstacles on the lattice chip and were collected at the outlets. We used NI-MAX and LabView to retrieve the pictures and manage the experimental instruments.

To described the separation results, we introduced a measure of the resolution defined as,

$$Rs = \frac{\mu_s - \mu_b}{2(\sigma_s + \sigma_b)} \quad (4)$$

Where μ_s is the average outlet number for small particles, which is obtained by adding up the probability of each outlet multiplied by the corresponding outlet number. As in the case of gravity, we only consider particles that move through the entire device. Similarly, we calculate the average outlet number for big particles, μ_b. $\boldsymbol{\sigma}_s$ is the standard deviation of outlet number for small particles, and $\boldsymbol{\sigma}_b$ is the standard

deviation of outlet number for big particles. Large resolution always denotes an effective separation.

Results and discussion

We found excellent separation at some specific angle for different types of particles. As to the cellulose acetate particles, at 15 and 20 degrees, their separation results were unsatisfying, while at 25 degrees, most small particles stayed in the Outlet 5 and 6 while most of larger ones went to the Outlet 7 and 8. As to the Delrin® acetal particles, at 15 and 25 degrees, the separation was not ideal, while a 20 degrees, most large particles moved in the displacement mode and exited the device at the left three outlets while most of the small particles crossed several columns of obstacles and moved in the zig-zag mode to right-side outlets.

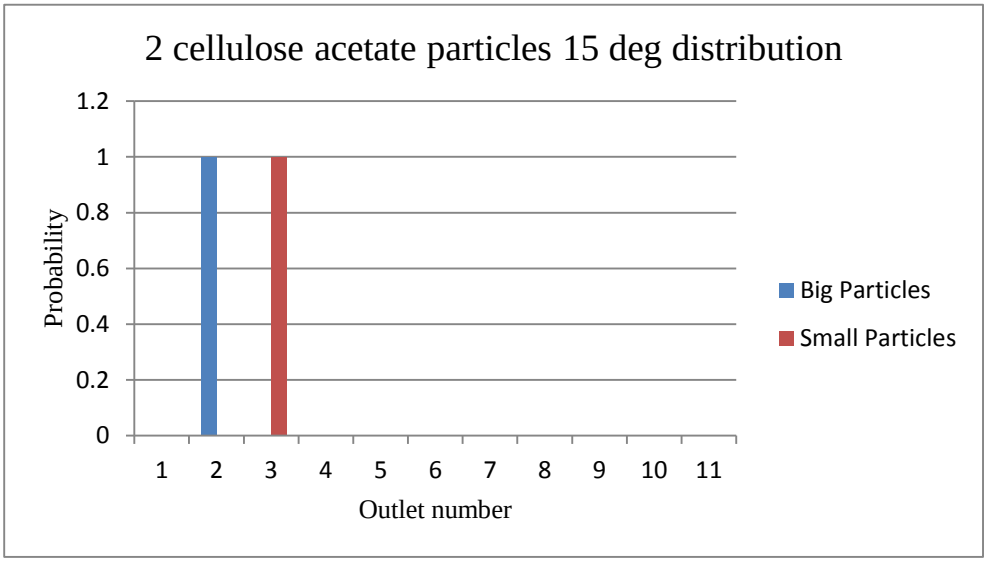

Fig.11 (a)

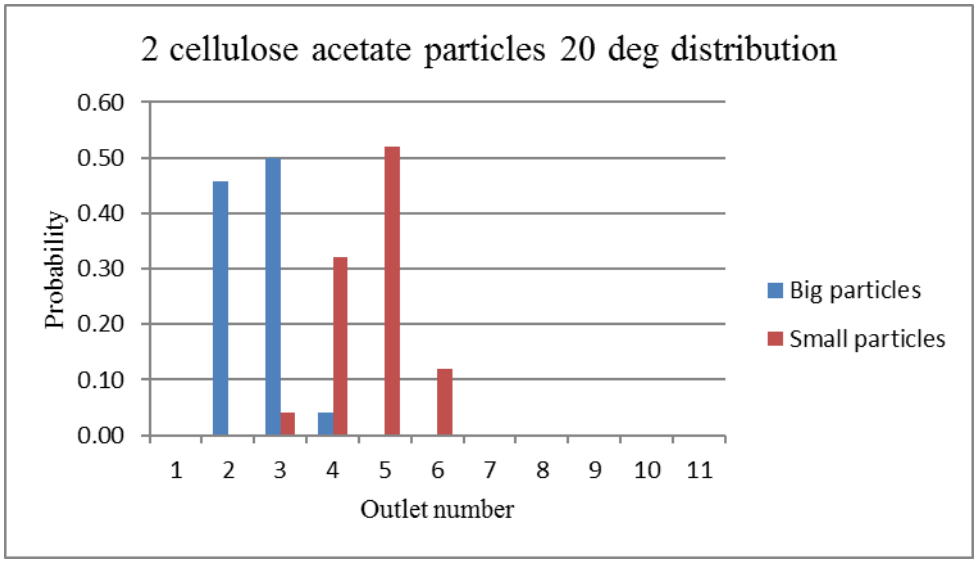

Fig.11 (b)

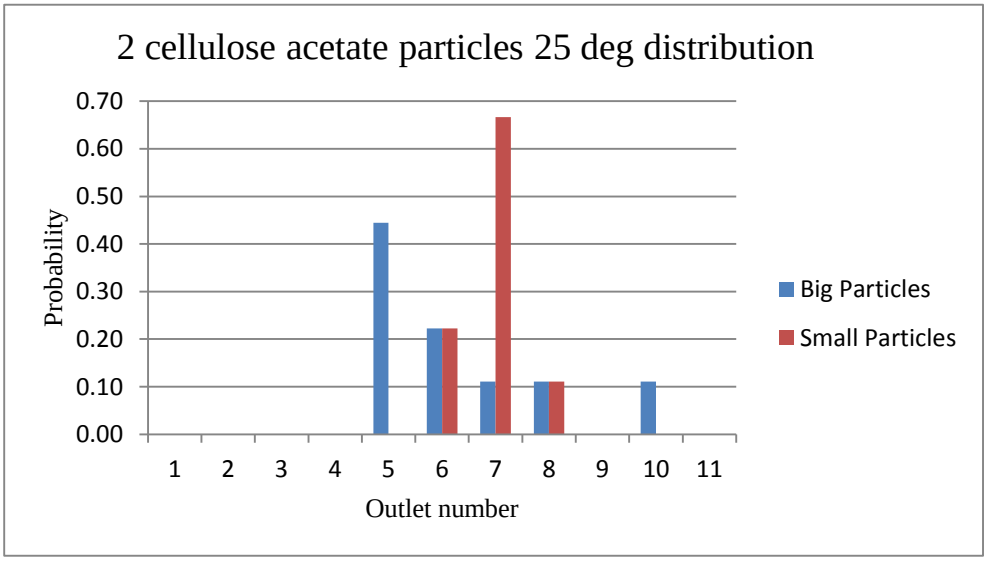

Fig.11 (c)

Fig.11 (a)~(c) Probability distribution for 2 cellulose acetate particles at forcing angles of 15, 20 and 25 degrees. The horizontal axis is the outlet number, the vertical axis shows the probability of particles collected in the corresponding outlet.

We performed 10 trials for 2 cellulose acetate particles at 15 degrees. The two types of particles were completely separated. All the large particles whose diameter is 1.50mm went to Outlet 2 and all the small particles whose diameter is 1.00mm were collected at Outlet 3. The calculated resolution is infinite and a larger number of trials would be needed to estimate its actual value. We performed 64 trials for 2 cellulose

acetate particles at 20 degrees. The two types of particles were mostly separated. Over 95% of the large particles went to Outlet 2 and 3, and over 95% of the small particles were collected from Outlet 4 to 6. The calculated resolution is 0.90. We performed 10 trials for 2 cellulose acetate particles at 25 degrees. The separation was not clear. Large particles scattered from Outlet 5 to10 and small particles scattered from Outlet 6 to 8. The calculated resolution is 0.13.

Thus for 2 cellulose acetate particles group placement, as the forcing angles increase from 15 to 25 degrees, the resolution is decreasing.

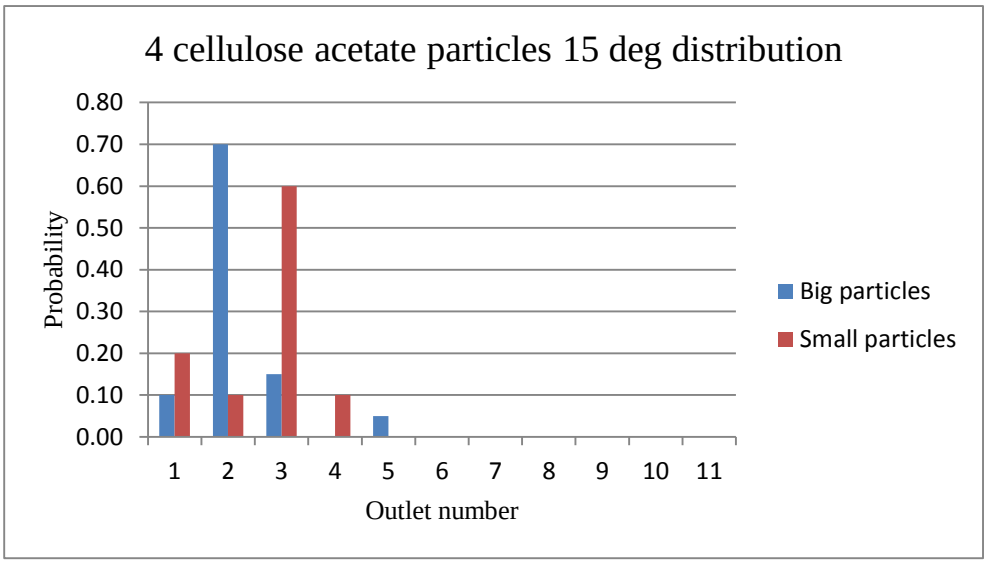

Fig.12 (a)

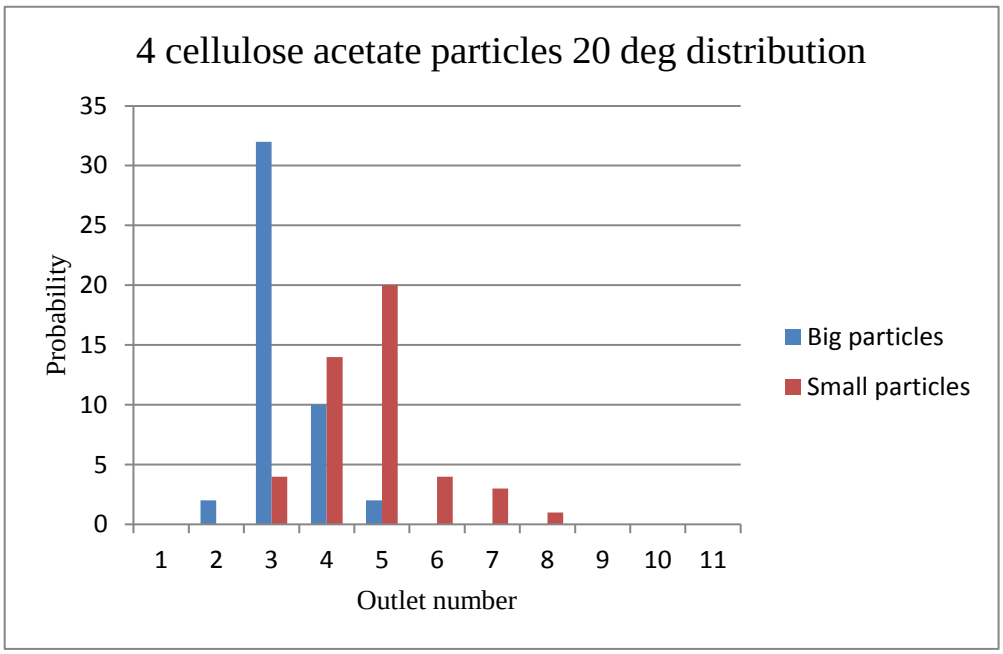

Fig.12 (b)

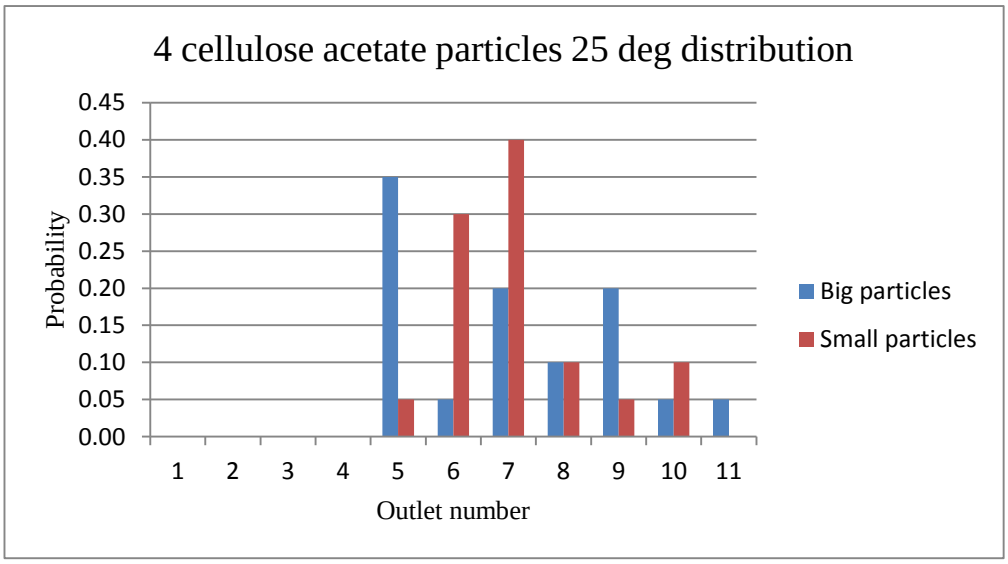

Fig.12 (c)

Fig.12 (a)~(c) Probability distribution for 4 cellulose acetate particles at forcing angles of 15, 20 and 25 degrees. The horizontal axis is the outlet number, the vertical axis shows the probability of particles collected in the corresponding outlet.

We performed 10 trials for 4 cellulose acetate particles at 15 degrees. The separation was not clear. Over 95% big particles went to Outlet 1 to 3 and all small particles scattered from Outlet 1 to 4. The calculated resolution is 0.12. We performed 25 trials for 4 cellulose acetate particles at 20 degrees. The separation was excellent.

Over 95% big particles went to Outlet 1 to 3 and over 95% small particles scattered from Outlet 4 to 8. The calculated resolution is 0.46. We performed 10 trials for 4 cellulose acetate particles at 25 degrees. The particles were not separated. The calculated resolution is 0.

Thus, for 4 cellulose acetate particles group placement at 15 and 25 degrees, they were not separated, while at 20 degrees, their separation was positive.

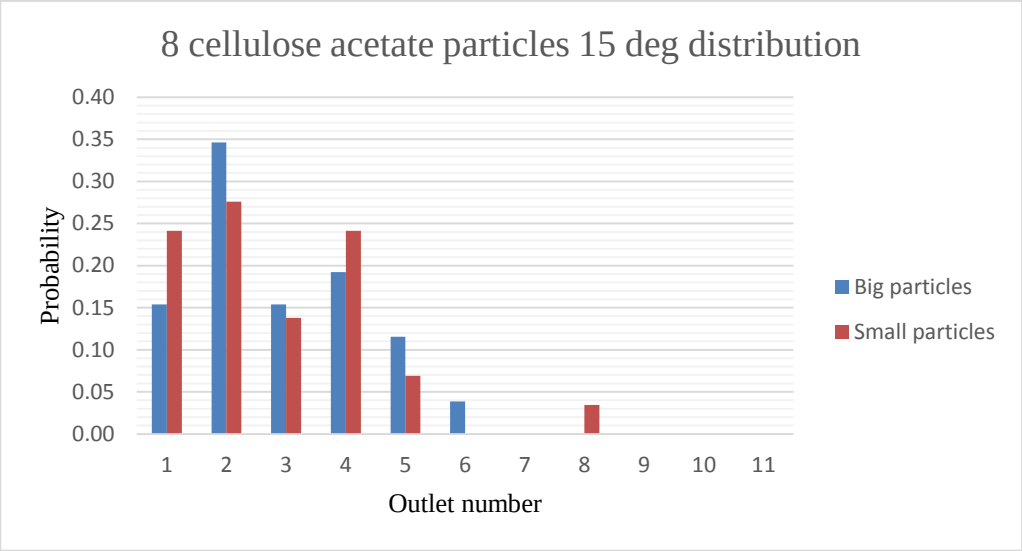

Fig.13 (a)

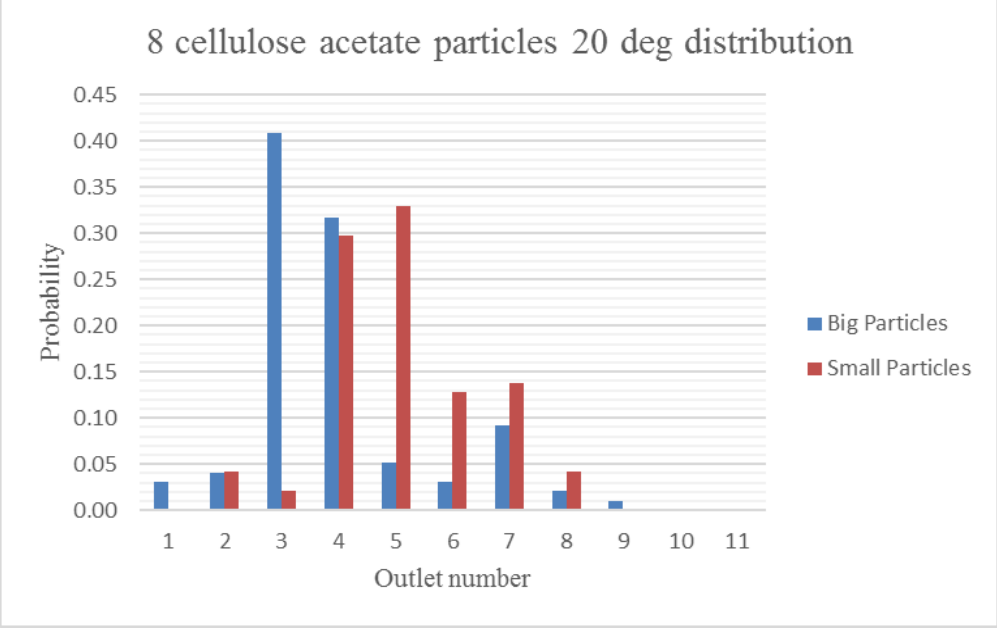

Fig.13 (b)

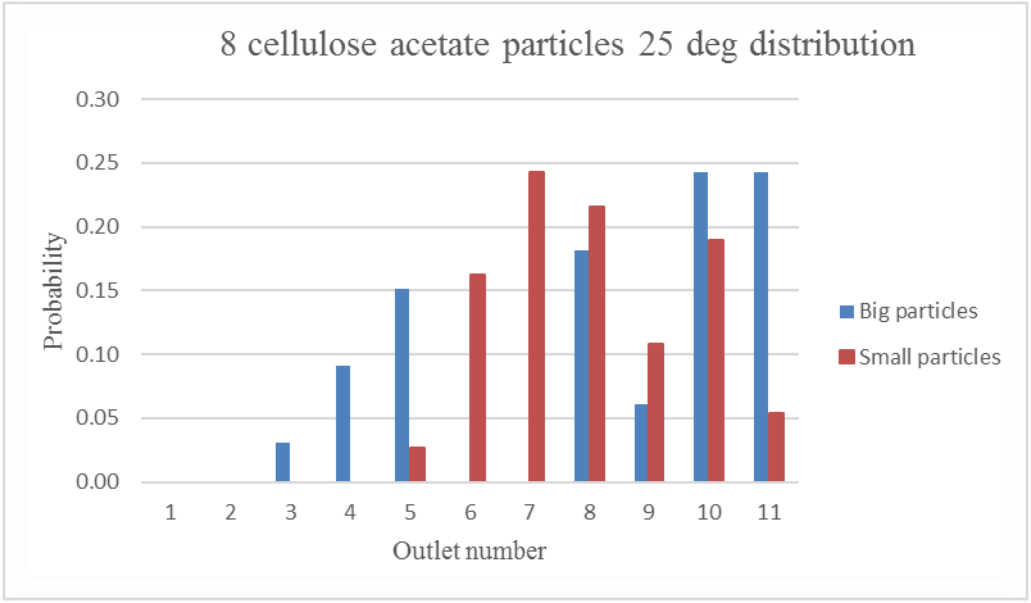

Fig. 13 (c)

Fig.13 (a)~(c) Probability distribution for 8 cellulose acetate particles at forcing angles of 15, 20 and 25 degrees. The horizontal axis is the outlet number, the vertical axis shows the probability of particles collected in the corresponding outlet.

We performed 10 trials for 8 cellulose acetate particles at 15 degrees. The particles were not separated. The calculated resolution is 0.02. We performed 25 trials for 8 cellulose acetate particles at 20 degrees. Over 75% big particles went to Outlet 1 to 4, and over 90% small particles went to Outlet 4 to 7. They were overlapped at Outlet 4. The calculated resolution is 0.19. We performed 10 trials for 8 cellulose acetate particles at 25 degrees. The calculated resolution is 0.03. They were not separated.

For 8 cellulose acetate particles at 15 and 25 degrees, the two types of particles were not separated. At 20 degrees, around 30% big particles and 30% small particles went to Outlet 4, thus the separation result was still not efficient.

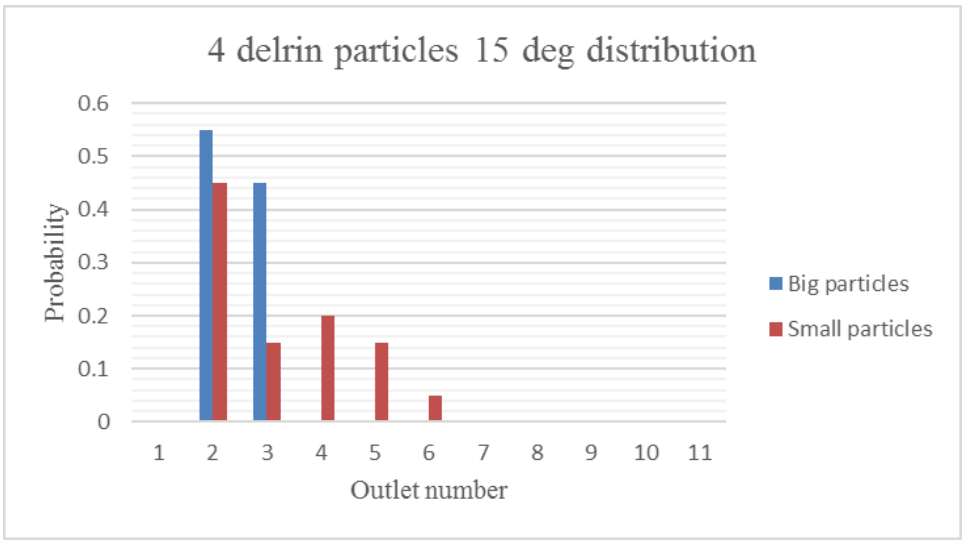

Fig.14 (a)

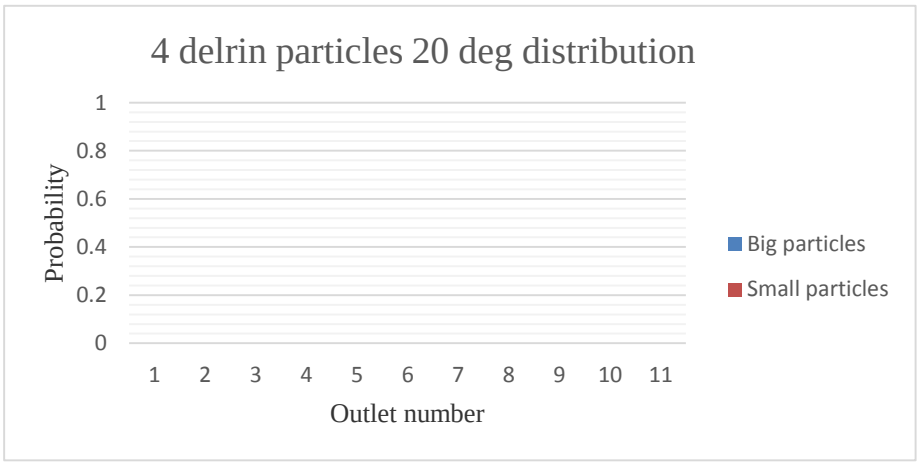

Fig.14 (b)

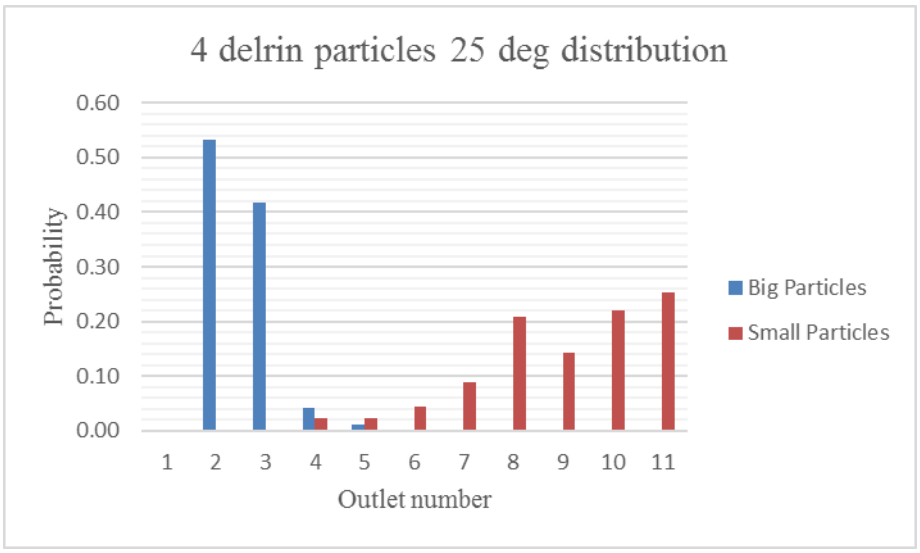

Fig.14 (c)

Fig.14 (a)~(c) Probability distribution for 4 Delrin® acetal particles at forcing angles of 15, 20 and 25 degrees. The horizontal axis is the outlet number, the vertical axis shows the probability of particles collected in the corresponding outlet.

We performed 10 trials for 4 Delrin® acetal particles at 15 degrees. All big particles went to Outlet 2 and 3, and small particles spread from Outlet 2 to 6. They were overlapped at Outlet 2 & 3. The calculated resolution is 0.21. We performed 10 trials for 4 Delrin® acetal particles at 20 degrees. All big particles went to Outlet 2 and 3, and small particles spread from Outlet 3 to 8. They were overlapped at Outlet 3. The calculated resolution is 0.50. We performed 50 trials for 4 Delrin® acetal particles at 25 degrees. Over 95% big particles went to Outlet 2 and 3, and small particles spread from Outlet 4 to 11. They were almost totally separated. The calculated resolution is 1.39.

Conclusion

We have shown that centrifugal force-driven deterministic lateral displacement has a great potential for separation of particles of different sizes. We

performed experiments in a scaled-up device which consists of patterned cylindrical posts. We investigated the relation between the distribution of particles at the outlet and the forcing angle. We noticed that the centrifugal force had effectively solved the problem of clogging and impediment in the device present in some earlier gravity driven DLD experiments, as discussed in the introduction to this part of the thesis. Our results have shown that for two, four and eight cellulose acetate particles placed together at the entrance of the array of obstacles and whose diameters are 1.00mm and 1.50mm, 20 degrees is a potential forcing angle for separation. For four Delrin® acetal particles initially released in group placement at the inner left corner of the device and whose diameters are 1.59mm and 2.38mm, 25 degrees is a potential forcing angle for separation. We also investigated the effect that the initial number of particles released together (or the initial concentration of particles) has on the separation and found that, for cellulose acetate, the smallest the initial number of particles we use, the better the separation resolution obtained in the experiments. Additional work should be done in the future to investigate the effects of interaction between particles on the separation results. In these experiments, at the first few seconds, particles were moving during the accelerating period of the centrifuge. Thus it will be more interesting to design a device where particles could be released after the centrifuge reaches a steady state.

Conclusions

We experimentally demonstrated that gravity-driven deterministic lateral displacement (g-DLD) has a great potential for separation of particles of different

shapes and sizes using scaled up devices. We also firstly proposed centrifuge-driven DLD devices for particles separation. In g-DLD experiments, we have shown that each type of particle starts to migrate at a given forcing angle. As the forcing angle increases, more and more particles migrate until at last all of them finally move across obstacle columns. The starting forcing angle increases with particle size for particles of the same shape. We also found that the critical angle is almost linear with respect to the diameter of the inscribed sphere, nearly independent of the specific particle shape. Thus, we could tell whether several different shapes of particles could be separated easily or not based on the difference between the diameters of their inscribed spheres. We also showed that the average migration angle is different for different particle shapes, which is the basis for their separation. We also compared the separation results for the spherical particles using two kinds of liquids of different viscosity. The results show that particles tend to migrate at a smaller starting forcing angle in more viscous fluid and display a sharper transition between no-migration and full-migration.

In the centrifuge-driven case, we noticed that the centrifugal force had effectively solved the problem of clogging and impediment which occurred in g-DLD devices. More important, our results demonstrate that cellulose acetate particles of two different sizes can be easily separated for a 20 degrees forcing angle. Similarly, 25 degrees seems to be a powerful forcing angle for separation for Delrin® acetal particles. We also noticed that for cellulose acetate particles, releasing a smaller number of particles together facilitate separation by improving resolution.

More work will be done to investigate the effects of viscosity of the fluid medium on separation of particles. In centrifuge-driven DLD experiments, particles start to move before the centrifuge reaches a steady state. Therefore, it will be interesting to design a device where particles could be released after the centrifuge reaches steady state, as this could have an impact on the resolution of the separation. In addition, more work should be done to explore the number of particles released on the separation efficiency.

Bibliography

1. Microfluidics: Fabrications and Applications. Luqmanulhakim Baharudin, Instrumentation Science & Technology, 2008, **36**, 222-230.
2. Microfluidics for biological applications. Wei-Cheng Tian, Erin Finehout, Springer, 2010.
3. Microfluidic DNA microarray analysis: A review. Lin Wang, Paul C. H. Li, Analytica Chimica Acta, 2011, **687**, 12-27.
4. Microfluidics: A focus on improved cancer targeted drug delivery systems. Ikram Ullah Khan, Christophe A. Serra *et al*, Journal of Controlled Release, 2013, **172**, 1065-1074.
5. Fabrication of a micro-direct methanol fuel cell using microfluidics. Chumphol Yunphuttha, Win Bunjongpru *et al*, Chemical Papers, 2012, **66**, 1137-1145.
6. Microfluidics for medical diagnostics and biosensors. Catherine Rivet, Hyewon Lee *et al*, Chemical Engineering Science, 2011, **66**, 1490-1507.
7. Microfluidics for cell separation. Ali Asgar S. Bhagat, Hansen Bow *et al*, Medical & Biological Engineering & Computing, 2010, **48**, 999-1014.
8. On-Chip Catalytic Microreactors for Modern Catalysis Research. Bin-Bin Xu, Yong-Lai Zhang *et al*, ChemCatChem, 2013, **5**, 2091-2099.
9. An Integrated Nanoliter DNA Analysis Device. Mark A. Burns, Brian N. Johnson *et al*, Science, 1998, **282**, 484-487.
10. Latest Developments in Micro Total Analysis Systems. Arun Arora, Giuseppina Simone *et al*, Analytical Chemistry, 2010, **82**, 4830-4847.
11. Continuous separation of cells and particles in microfluidic systems. Andreas Lenshof, Thomas Laurell, Chemical Society Reviews, 2010, **39**, 1203.
12. Electrical field-flow fractionation of proteins. K. D. Caldwell, J. C. Giddings *et al*, Science, 1972, **176**, 296-298.
13. Dynamic bioprocessing and microfluidic transport control with smart magnetic nanoparticles in laminar-flow devices. James J. Lai, Kjell E. Nelson *et al*, 2009, **9**, 1997.
14. Acceleration and trapping of particles by radiation pressure. A. Ashkin, Physical Review Letters, 1970, **24**, 159.
15. Selection of mammalian cells based on their cell-cycle phase using dielectrophoresis. Unyoung Kim, Chih-Wen Shu *et al*, 2007, **104**, 20708–20712.
16. Magnetism and microfluidics. Nicole Pamme, Lab on a Chip, 2006, **6**, 24.
17. Separation of lipids from blood utilizing ultrasonic standing waves in microfluidic channels. Filip Petersson, Andreas Nilsson *et al*, The Analyst, 2004, **129**, 938.
18. Continuous particle separation through deterministic lateral displacement. L. R. Huang, Science, 2004, **304**, 987-990.
19. Hydrodynamic filtration for on-chip particle concentration and classification utilizing microfluidics. Masumi Yamada, Minoru Seki, Lab on a Chip, 2005, **5**, 1233.
20. Pinched flow fractionation: Continuous size separation of particles utilizing a laminar flow profile in a pinched microchannel. Masumi Yamada, Minoru Seki, Lab on a Chip, 2004, **76**, 5465-5471.

21. Continuous inertial focusing, ordering, and separation of particles in microchannels. Dino Di Carlo, Daniel Irimia *et al*, Proceedings of the National Academy of Sciences, 2007, **104**, 18892–18897.
22. Gravity Driven Deterministic Lateral Displacement for Particle Separation in Microfluidic Devices. Raghavendra Devendra, German Drazer, Analytical Chemistry, 2012, **84**, 10621-10627
23. Improved performance of deterministic lateral displacement arrays with triangular posts. Kevin Loutherback, Kevin S. Chou *et al*, 2010, **9**, 1143-1149.
24. New design for the separation of microorganisms using microfluidic deterministic lateral displacement. Mohamed Al-Fandi, Mohammad Al-Rousan *et al*, 2011, **27**, 237-244.
25. Chiral Particle Separation by a Nonchiral Microlattice. Lukas Bogunovic, Marc Fliedner et al, Physical Review Letters, 2012, **109**,100603.
26. Separation of deformable particles in deterministic lateral displacement devices. Raymond Quek, Duc Vinh Le et al, Physical Review E, 2011, **83**, 056301.
27. Sorting cells by size, shape and deformability. Jason P. Beech, Stefan H. Holm *et al*, Lab on a Chip, 2012, **12**, 1048.
28. Inertia and scaling in deterministic lateral displacement, Timothy Bowman, German Drazer, Joelle Frechette, Biomicrofluidics, 2013, **7**, 064111.
29. Trajectory and distribution of suspended non-Brownian particles moving past a fixed spherical or cylindrical obstacle. Sumedh R. Risbud, German Drazer, Journal of Fluid Mechanics, **714**, 213-237.
30. Directional locking in deterministic lateral-displacement microfluidic separation systems. Physical Review E, 2014, **90**, 012302.
31. Force driven separation of drops by deterministic lateral displacement. Timothy Bowman, Joelle Frechette, German Drazer, Lab on a Chip, 2012, **12**, 2903-2908.
32. Shape separation of nanometer gold particles by size-exclusion chromatography. Guor-Tzo Wei, Fu-Ken Liu *et al*, Analytical Chemistry, 1999, **71**, 2085-2091.
33. Physical approaches to biomaterial design. Samir Mitragotri, Joerg Lahann, Nature Materials, 2009, **8**, 15-23.
34. Assessment of erythrocyte shape by flow cytometry techniques. M Piagnerelli, K Zouaoui Boudjeltia *et al*, Journal of Clinical Pathology, 2006, **60,** 549-554.
35. Nanoparticle-mediated cellular response is size-dependent. Wen Jiang, Betty Y. S. Kim *et al*, Nature Nanotechnology, 2008, **3**, 145-150.
36. Shape-dependent compressibility of TiO2 anatase nanoparticles. Seung-won Park, Jung-tak Jang *et al*, The Journal of Physical Chemistry C, 2008, **112**, 9627-9631.
37. Observation of nonspherical particle behaviors for continuous shape-based separation using hydrodynamic filtration. Sari Sugaya, Masumi Yamada *et al*, Biomicrofluidics, 2011, **5**, 024103.
38. Tipping the balance of deterministic lateral displacement devices using dielectrophoresis. Jason P. Beech, Peter Jönsson *et al*, Lab on a Chip, 2009, **9**, 2698.